Clays and Clay Minerals, Vol. 44, No. 1, 49–67, 1996.

ALTERATION OF SILICIC VITRIC TUFFS INTERBEDDED IN VOLCANICLASTIC DEPOSITS OF THE SOUTHERN BASIN AND RANGE PROVINCE, MEXICO: EVIDENCES FOR HYDROTHERMAL REACTIONS

PHILIPPE MÜNCH, JOËLLE DUPLAY,[1] AND JEAN-JACQUES COCHEMÉ[2]

Laboratoire de Pétrologie Magmatique, U.R.A. C.N.R.S. 1277, Faculté St. Jérôme
Université Aix-Marseille III, 13397 Marseille cedex 20, France

[1] Centre de Géochimie de la Surface, CNRS, 1 rue Blessig, 67084 Strasbourg cedex, France

Abstract—In Northwestern Mexico, the Miocene basins that disrupted the Sierra Madre Occidental Province are filled with sandstones and conglomerates (the Báucarit Formation) cemented mainly by zeolites of the heulandite-clinoptilolite group. Few volcanic tuffs are intercalated in the sediments for which four different groups of samples have been defined. These groups correspond to a gradation in the alteration of the glassy matrix. Group 1 is characterized by the preservation of the glassy matrix and the presence of disseminated patches of clay minerals with a continuous variation between aluminous Al-montmorillonite and ferric smectite end-members. Heulandite-group zeolites and opal C-T are also present. Group 2 is characterized by a nearly complete replacement of volcanic glass by a more homogeneous Al-montmorillonite. In some samples, heulandite-group zeolites are present as clusters on clay minerals. The primary vitroclastic texture is generally preserved and relict glass is present in small amounts. In group 3, the secondary assemblage is dominated by heulandite-group zeolite crystals as pseudomorphs of shards and pumiceous fragments. Discrete illite is present in all samples. Textures are exceptionally well-preserved. Group 4 is characterized by the presence of heulandite and clay minerals in which the Mg-Fe smectite end-member is more magnesian than in other groups. The original texture is not preserved.

The following are deduced from the mass-balance calculations: the alteration of the tuffs leads to a strong Mg- and Ca- and, to a lesser degree, Fe-enrichment, and to Na and K depletion. Zeolites account for Ca-enrichment and clay minerals are host for Fe and Mg. As a consequence, alteration may have occurred under open system conditions and the most likely source for the high Ca and Mg gains is a fluid circulating through the underlying volcaniclastic sediments and underlying mid-Tertiary volcanics of the bimodal (basaltic-rhyolitic) sequence. However, those fluids may have been rather dilute and weakly alkaline.

As estimated temperatures are between 85 and 125°C and as there is only a low burial, it is proposed that hot fluids are responsible for the alteration of volcanic glass. A decrease with time in the initial permeability of the tuffs is consistent with the observed evolution of the changing Al-smectite toward a more magnesian composition.

Key Words—Basin and Range, Hydrothermal alteration, Mass-balance calculations, Mexico, Smectites, Transmission electron microscopy, Volcanic tuffs, Zeolites.

INTRODUCTION

In a previous paper, Münch and Cochemé (1993) questioned the meaning of the zeolites found as a cement in the Miocene molassic deposits from the southern Basin and Range (Sonora Province, Mexico). It was suggested that a steep geothermal gradient, enhanced by lithospheric thinning may have been responsible for heulandite crystallization. As preserved volcanic tuffs were found at different stratigraphic levels in few basins, we now address, in this paper, their grade of alteration. Moreover, few studies have been made on the alteration of vitric tuffs using transmission electron microscopy (TEM) and analytical electron microscopy (AEM) techniques. The objectives of the study are: 1) to characterize the texture, mineralogy and chemistry of tuffaceous rocks using X-ray diffraction (XRD), electron microprobe analysis (EPMA), scanning electron microscopy (SEM) and bulk rock analysis; 2) to apply TEM and AEM analysis to the study of glass alteration within the samples in order to examine at a fine scale the chemistry of the coexisting secondary minerals; 3) to estimate compositional changes from glass to zeolites and/or clay minerals; and 4) to identify the processes involved in the alteration.

GEOLOGICAL SETTING

The state of Sonora, Mexico, belongs to the southwestern extremity of the Basin and Range physiographic province. In this region, a pre-Basin and Range extensional phase (Zoback et al. 1981) is coeval with a bimodal volcanism, well exposed throughout the Northern Sierra Madre Occidental province (Demant et al. 1989). Thus, an extensional episode resulted in the formation of numerous, elongated, NNW–SSE trending, intermontane basins that have a basement of mid-Tertiary volcanics. The basins were

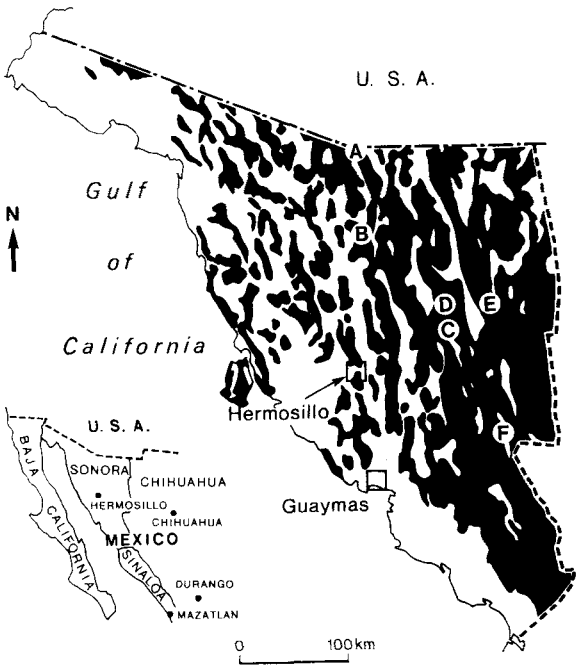

Figure 1. Sample location map with black areas corresponding to ranges and white ones to basins. Open circles indicate basins from which samples were collected: A, sample 90-16; B, sample 45-89; C, sample 43-89; D, samples S-88-1, S-88-2, S-88-3 and 90-2a; E, S-88-6; F, 90-8a. The names of the localities are given in Table 1.

filled by volcaniclastic sediments of fine-grained sandstones to conglomerates, deposited as overlapping and coalescing alluvial fans. Volcanic rocks, mainly basalt flows and scarce, thin and white silicic ash beds, are interbedded with sediments at different levels in the series. Tuffaceous rocks range from stratified ash-fall tuffs to reworked pumiceous tuffs. Those paleo-basin infill sediments are now well indurated and are easily recognized as they form pillars and pinnacles. They were named the Báucarit Formation by King (1939). Most outcrops of the Báucarit Formation are located at the western foothills of the Sierra Madre Occidental province. The maximum observed thickness of this formation does not exceed 400 m. The age of the sediments is constrained as they overlay basalts dated at 17.6 My in the region of Yécora (Bockoven 1980) and as they underlie volcanic rocks dated around 14 My (Drewes 1981; Bartolini et al. 1992). The presence of heulandite, as a cement, within sandstones was pointed out by Cochemé et al. (1988). The zeolites responsible for the lithification of the sediments have been studied by Münch and Cochemé (1993). The Báucarit Formation was faulted during the main Basin and Range extensional phase (Zoback et al. 1981). The basin infill has continued to the Pliocene except in the Sierra Madre Occidental province.

SAMPLING AND METHODS

Ash beds within the Báucarit Formation are scarce. We sampled six basins where tuffaceous rocks were found at different levels in the sedimentary sequence (Figure 1). The localities, the stratigraphic position and the petrographic description of all samples are given in Table 1.

Zeolites were analyzed by electron microprobe (EPMA) at the University of Montpellier with an accelerating voltage of 20 kV, a sample current of 10 nA and a beam diameter of 10 μm. Zeolite analyses were selected based on their low chemical balance E% =

Table 1. Localities, sample description and stratigraphic position.

Sample #	Basin	Localities	Sample description	Stratigraphic position
90-16	A	Agua Fria Cañon, Nogales (USA).	Ash flow Tuff, 2 m thick, white, rich in rhyolitic fragments.	Near the top of the Báucarit Formation, underlying a basaltic flow dated at 13.5–13.8 Ma (Drewes 1981).
45-89	B	Pueblo Magdalena, Sonora.	Ash fall tuff, 10 cm thick, white.	Intermediate position, interbedded within volcaniclastic sandstones.
43-89	C	Rancho La Montosa, Huepari	Reworked pumiceous tuff, thickness not determined, white.	Intermediate position, interbedded within volcaniclastic sandstones.
S-88-2	D	Rancho El Colador, Mazocahui, Sonora.	Ash fall tuff, 15 cm thick, white, stratified, vitroclastic texture.	Intermediate position, interbedded within volcaniclastic sandstones.
90-2a		Rancho El Colador, Mazocahui, Sonora.	Ash fall tuff, 10–15 cm, yellowish	Intermediate position, interbedded within volcaniclastic sandstones.
S-88-3		Rancho El Colador, Mazocahui, Sonora.	Ash fall tuff, 10 cm thick, white.	Intermediate position, interbedded within volcaniclastic sandstones.
S-88-1		Rancho El Colador, Mazocahui, Sonora.	Pumiceous tuff, moderately reworked, thickness less than 1 m, white.	Intermediate position, interbedded within volcaniclastic sandstones.
S-88-6	E	Pueblo Huasabas, Sonora.	Ash fall tuff, 30–40 cm thick, white, vitroclastic texture.	Intermediate position, interbedded within volcaniclastic sandstones.
90-8a	F	Tepoca, Sonora State.	Reworked tuff, variable thickness (>1 m), yellowish.	At the bottom of a basin, overlying mid-Tertiary volcanics.

https://doi.org/10.1346/CCMN.1996.0440105 Published online by Cambridge University Press

Table 2. Characteristics and secondary mineralogical assemblages in altered tuffs interbedded in the Báucarit Formation, Sonora, Mexico.

Facies from this study	Sample #	Alteration state and secondary minerals (listed by decreasing abundance*)
Group 1	90-16	Fresh volcanic glass, smectites, opal C-T and intermediate heulandite
Group 2	45-89, S-88-6 S-88-2	Smectites, intermediate heulandite and traces of altered glass
Group 3	90-2a, S-88-3 S-88-1, 43-89	Clinoptilolite and/or intermediate heulandite, I/S minerals with 70% expandable layers and significant amount of illite; volcanic glass has been completely dissolved
Group 4	90-8a	Heulandite and I/S minerals with 80% expandable layers

* Mineralogy determined by X-ray diffraction of bulk rock powder.

100[Al − (Na + K) − 2(Ca + Mg + Sr + Ba)]/[Na + K + 2(Ca + Mg + Sr + Ba)], defined by Passaglia (1970). Only analyses with E < 10% were accepted.

The samples were examined on a Philips CM12 analytical electron microscope and chemical analyses were performed using an X-ray energy dispersive detector (EDAX PV9900). The X-ray spectra were acquired during 100 seconds with no Be window. Chemical analyses were obtained by STEM mode only for areas that were observed by TEM mode and characterized by SAED. Corrections were made using a standard for thin films (Cliff and Lorimer 1975). Analytical errors in the concentrations are estimated of the order of 2% for major elements and 5 to 10% for minor elements. Major element analyses, except alkalis, of bulk samples were made with an I.C.P. spectrometer. Alkalis were analyzed by atomic adsorption.

X-ray powder diffraction (XRD) analyses were performed on a Philips PW1710 diffractometer equipped with a Co tube and a carbon monochromator. The <2 μm fraction was obtained by centrifugation and sedimented onto glass slides, which were used to determine the clay mineralogy after ethylene-glycol treatment and heating. The estimation of the percentage of expandable layers for illite/smectite interstratified minerals was made with the saddle/001 method (Weir et al. 1975; Rettke 1981). The thermal stability of heulandite-group zeolites was checked by XRD analysis of bulk rock powders heated at 450°C for 15 h (Mumpton 1960).

RESULTS

MINERALOGICAL RESULTS. From petrographic observations, glass was the main primary component (>95 vol%) of the tuffs which are characterized by the same primary mineral assemblage: plagioclase, biotite, alkali feldspar, and quartz in order of decreasing volume abundance. These minerals have been observed as fragmented microphenocrysts (<1 mm) and do not show any petrographic evidence of alteration. In the most reworked samples, subrounded or rounded acidic volcanic rock fragments have also been noted. Different secondary mineralogical assemblages have been recognized allowing us to define four distinct groups of samples (Table 2). These groups correspond to a progressive increase in glass alteration and are consistent with the relative stratigraphic heights of samples.

Group 1 is characterized by extensive preservation of primary volcanic glass within tuffs and correspond to the top of the Báucarit Formation. Unfortunately only one tuff layer (sample 90-16) was found within the upper part of the sedimentary sequence. Glass alteration is restricted to limited patches disseminated within the groundmass of tuffs. The secondary mineralogy is dominated by smectite and includes heulandite-group minerals classified as intermediate heulandite (heulandite-B has formed after heating overnight at 450°C), and opal.

SEM observations showed that interstratified illite/smectite (I/S) has a cornflake morphology typical of smectite or I/S minerals with high expandable layers (Keller et al. 1986). Opal occurs as spheres or hemispheres with short, stubby and radiating crystals growing on glass surface (Figure 2a). Heulandite-group zeolites occur as euhedral crystals with the characteristic tabular shape, some of which are coffin-shapped crystals.

TEM observations of dispersed clay particles showed that the clay minerals have a flaky to slightly platy morphology (Figure 3a). High-magnification lattice fringe images of ultra-thin sections show packets of layers, about 50 Å thick, with mottled contrast (Figure 3b). The measured periodicity of these layers is about 10 Å. However, minor areas with discontinuous wavy layers of variable periodicity, have also been observed (arrow on Figure 3b).

Groups 2 and 3 correspond to the intermediate part of the sedimentary sequence. Both are characterized by the nearly complete alteration of volcanic glass. Hence, they have been distinguished on the basis of their secondary mineralogical assemblages and not based on their relative stratigraphic position.

Group 2 (samples 45-89, S-88-6 and S-88-2) is characterized by nearly complete replacement of volcanic glass and by smectite-dominated mineralogy. Smectite comprises 60–95 vol% of altered tuffs from this group (sample 45-89) and has the highest smectite

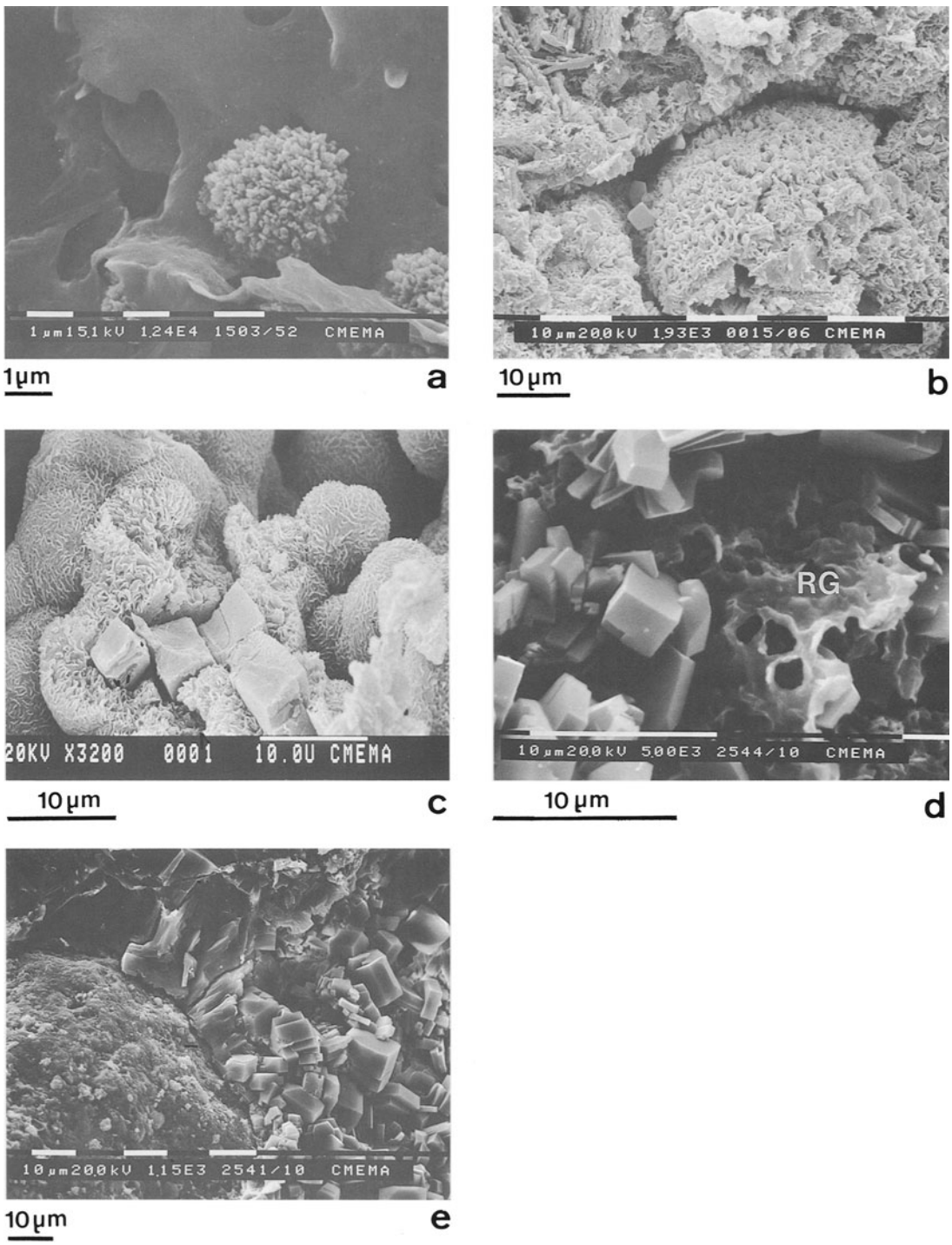

Figure 2. SEM secondary electron images of altered tuffs from the Báucarit Formation, Sonora State, Mexico. a) An opal-CT sphere developed onto fresh glass from the sample 90-16. b) A platy bubble-wall shard dissolved and outlined by smectites and heulandite-group zeolites from the sample S-88-6 (group 2). c) Rounded masses of smectite from the sample 45-89 surrounding magmatic plagioclases at the center of the picture (group 2). d) Heulandite-group zeolites onto remaining altered glass from the sample S-88-2 (group 2). RG: relict glass. e) Clinoptilolite crystals filling vug and showing a corona-like arrangement onto detrital grain from the sample 43-89 (group 3).

https://doi.org/10.1346/CCMN.1996.0440105 Published online by Cambridge University Press

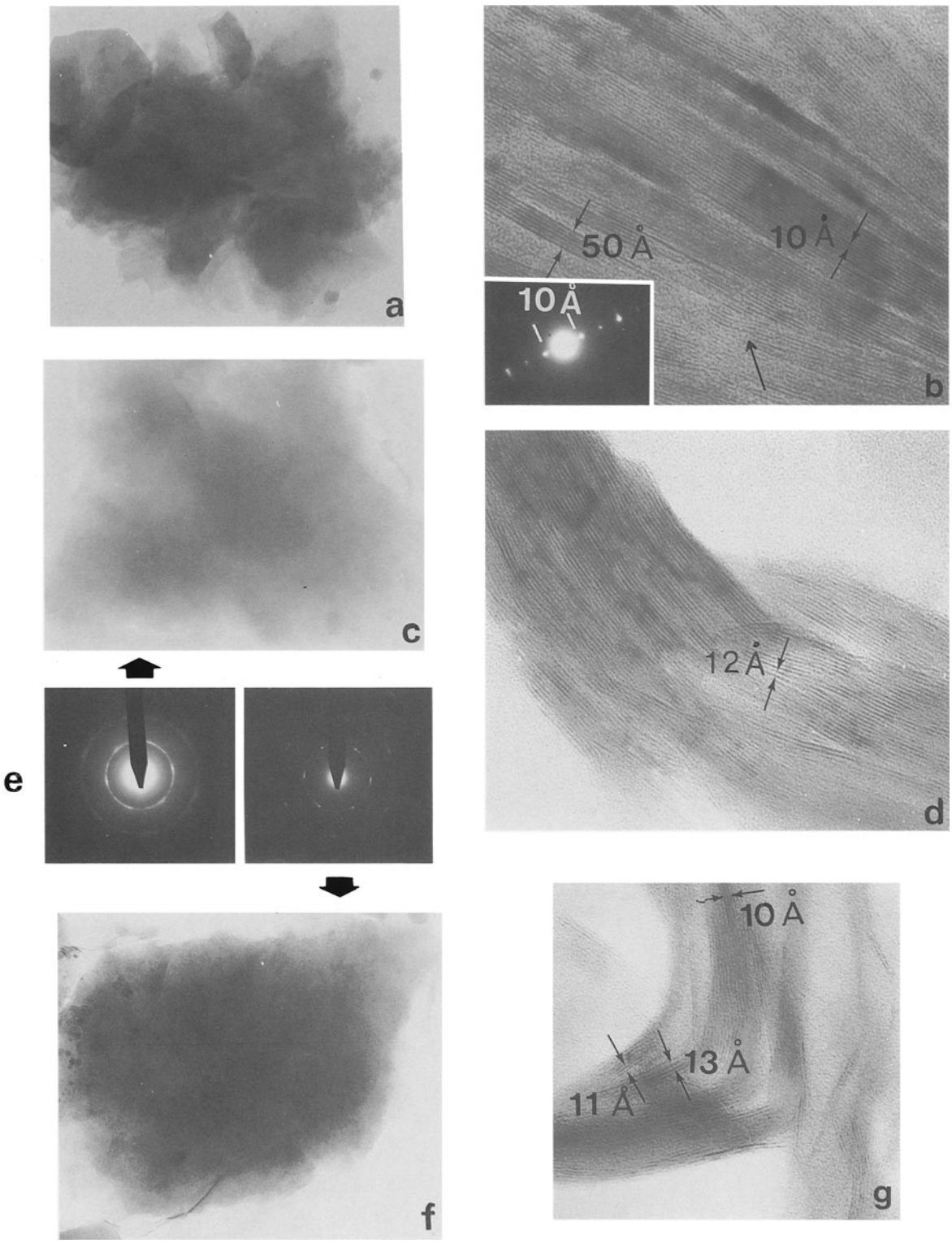

Figure 3. TEM images of the clay fraction (<2 μm) showing various clay morphologies and lattice fringe images. a) TEM image of clay particles from sample 90-16 showing a flacky to platy morphology. b) High-resolution lattice fringe of ultrathin section showing mottled contrast and a periodicity near 10 μ (sample 90-16). c) TEM image of typical smectite flacke-like particles from sample S-88-6 (group 2). d) High-resolution lattice fringe image showing the disordered structure of smectite with many edge dislocations. e) SAED patterns of smectites (samples S-88-6 and 90-8a). f) TEM image of clay particles from sample 90-8a (group 4) showing a platy to flacky morphology. g) High-resolution lattice fringe image of bended smectite layers of variable periodicity (sample 90-8a).

https://doi.org/10.1346/CCMN.1996.0440105 Published online by Cambridge University Press

content, which is now a bentonite. The mineralogy also includes heulandite-group zeolites and their abundance is inversely related to that of smectite. Petrographically, these tuffs are composed of more than 95 vol% of a fine-grained matrix formed by intimately intermixed smectites and zeolites. Rare clusters of large zeolite crystals have been noted.

XRD analysis of sample 45-89 revealed the presence of pure dioctahedral smectite (determined with the 060 peak position) with no interstratified illite layer. In other samples interstratified I/S with 70–86% expandable layers have been recognized (Figure 5). Heulandite-group minerals have been determined as intermediate heulandite.

The primary vitroclastic texture of tuffs is poorly preserved, but platy bubble-wall shards have been observed with the SEM (Figure 2b). Rounded masses of smectite have also been noted within sample 45-89 (Figure 2c). SEM observations have shown relict glass within altered tuffs from this group (Figure 2d). The zeolites are developed onto clays in voids created by glass dissolution (Figure 2d). Thus, intermediate heulandite has been formed later than smectites.

TEM images of the clays from two different samples (S-88-2 and S-88-6) showed that the particles generally have a flaky morphology (Figure 3c). On high-resolution lattice fringe images of ultra-thin sections, clay particles exhibit a typical wavy and discontinuous smectite texture (Figure 3d). In sample S-88-2, the smectite packets are sometimes disseminated in a non-crystalline substrate and their thickness is limited to a few layers only. The best observed texture is pointed out for sample S-88-6 where packets of layers (Figure 3d) are more extended in thickness and less discontinuous.

Group 3 (samples 90-2a, S-88-3, S-88-1 and 43-89) is characterized by a heulandite-group zeolites dominated mineralogy. These zeolites, which are associated with clay minerals, make up 80–90 wt% of the altered tuffs. They occur both as clusters of euhedral crystals within interstices and as pseudomorphs of shards and pumiceous fragments. Zeolite crystals grow perpendicular to the walls of interstices between shards, pumiceous and rock fragments (Figure 2e). The interiors of glassy fragments are filled by randomly oriented, large crystals. Clay minerals form a thin coating, a few micrometers thick, on the surface of replaced glass fragments.

From XRD analysis of bulk rock powders, the samples from this group are nearly pure heulandite-group zeolite. Heat treatment of zeolites revealed the presence of clinoptilolite and/or intermediate heulandite in these samples. In sample 43-89 the two thermal behaviors (contracted and unchanged 020 peak) have been recognized. Smectite is randomly interstratified with illite and the calculated percentage of smectite layers is 70–80%. Discrete illite has also been noted in all samples from this group, especially in sample 43-89 (Figure 5).

SEM observations showed that vitroclastic texture and glass have been rarely preserved. Interstratified I/S and heulandite-group zeolites have similar morphologies to those in samples from group 2.

In samples 43-89 and 90-2a, three morphological clay types can be identified with TEM. The first type is similar in morphology to the smectites of samples from group 2. The particles are flaky, thin, and curved (Figure 4a). They contain abundant crystal defects and the layer periodicity varies from 10 to 16 Å (Figure 4a, b and c). The texture is turbostratic (Figure 4b). The second type exhibits a thin platy and elongated shape (Figure 4d). The layers are subparallel with a periodicity of about 10–11 Å (Figure 4e). The SAED patterns of this second type show a quite high degree of order, as indicated by the presence of hkl diffraction spots (Figure 4b). The third type corresponds to well-crystallized clay minerals with a platy shape and sharp edges (Figure 4f). The layer packets are subparallel and almost defect-free. The main observed periodicity is 10 Å but slight variation can also be observed (Figure 4g and h). These appear to be subhedral illite-type crystals.

Group 4, characterized by the presence of heulandite sensu stricto (complete destruction of the 020 peak reflexion), is represented by only one sample (sample 90-8a), which is located at the base of the sedimentary sequence. Clay minerals, identified as randomly interstratified I/S with 80% expandable layers, are very abundant and occur as a matrix disseminated throughout the sample.

SEM observations showed that morphologies of both heulandite and interstratified I/S are similar to those in other groups. Neither relict texture nor relict glass was observed.

The clays from sample 90-8a have a platy to flaky particle morphology in a disordered arrangement (Fig-

→

Figure 4. TEM images of the clay fraction (<2 μm) showing various clay morphologies and lattice fringe images. a) TEM image of an Al-rich smectite flake with curling on its edges and a turbostratic layer arrangement (b). b) SAED pattern of aluminous and ferromagnesian smectites. c) High-resolution lattice fringe image of a typical curved and disordered layer structure of the Al-rich form. d) Lath-like, elongated shape of an Mg, Fe-rich smectite particle with well-ordered structure as suggested by SAED pattern (b). e) High-resolution image of the layer arrangement in an Fe-rich smectite. f) TEM image of illite with a polyhedral shape and sharp edges. g) High-resolution image showing illite layers with typical ordered structure with parallel layers and a periodicity of 10 Å h) High-resolution image of slightly expandable illite.

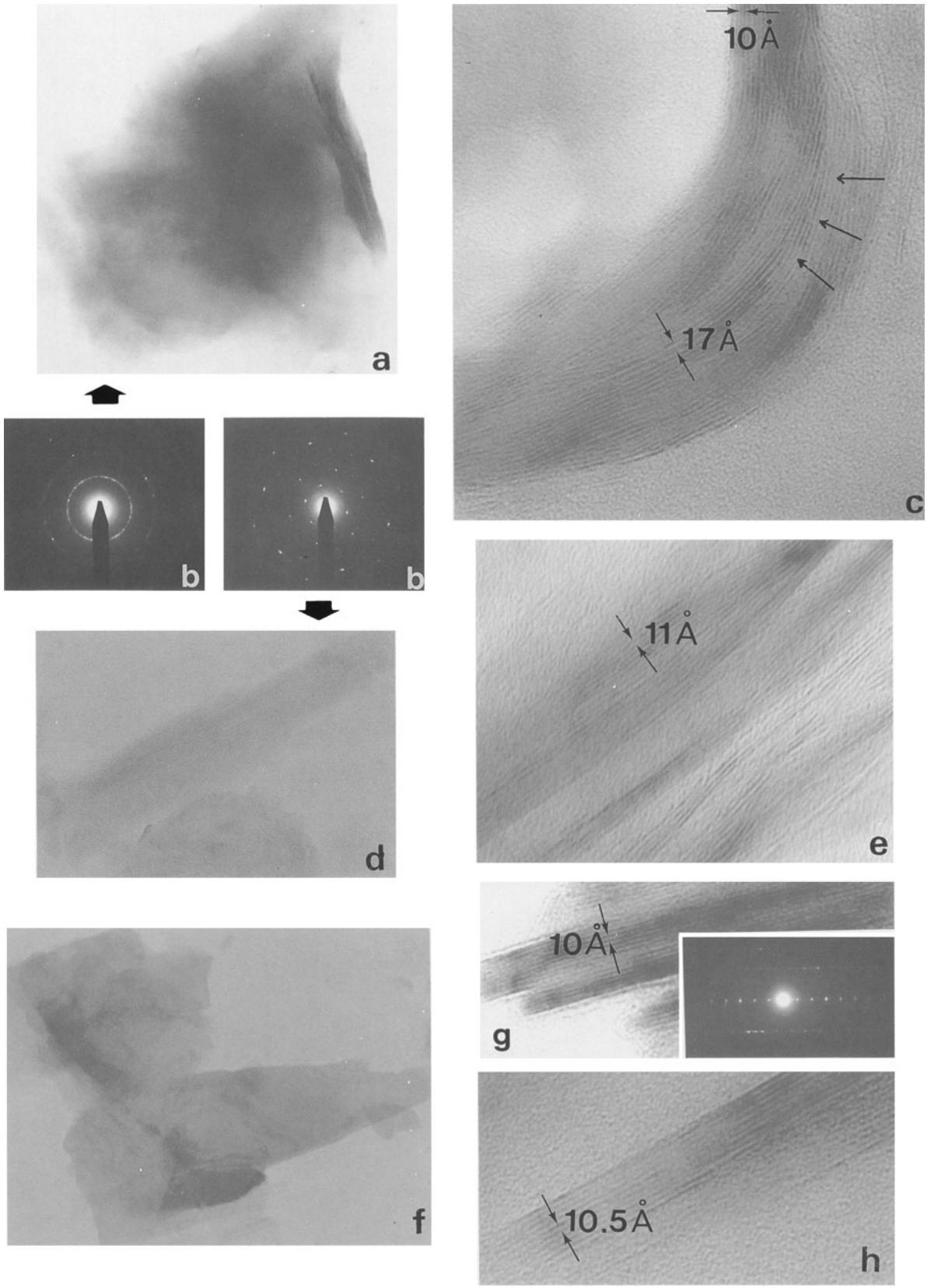

https://doi.org/10.1346/CCMN.1996.0440105 Published online by Cambridge University Press

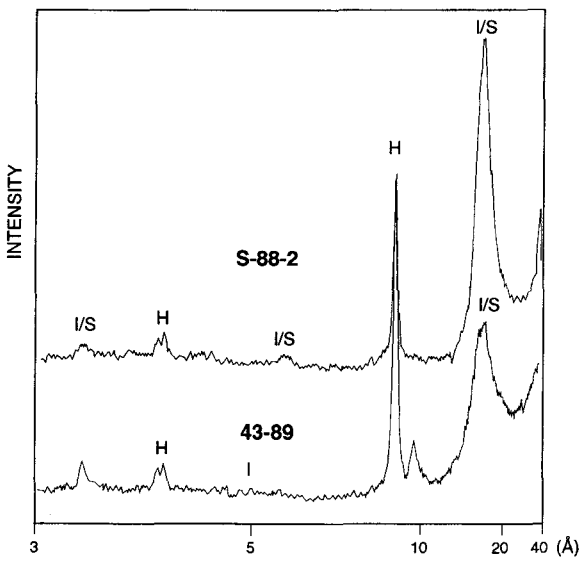

Figure 5. X-ray diffraction patterns of two glycolated samples (<2 μm fraction): a) Sample S-88-2 (90% mixed-layer illite); and b) Sample 43-89 (70% mixed layer illite). I/S = randomly interstratified illite/smectite minerals; I = authigenic illite; H = heulandite-group zeolite.

ure 3f). The lattice fringe image shows bended smectite layers of variable periodicity from 11 to 13 Å (Figure 3g) with limited areas of 10 Å periodicity inserted into it. However the layer periodicity is variable, while rigid packets of layers are intercalated with more flexible layers characterizing an interstratified arrangement (Figure 3g). This morphology is similar to that of rigid layers interstratified with typical smectites from Group 3 samples.

Chemical Results

EPMA. The glass from sample 90-16 has a rhyolitic composition (Table 3). The chemical compositions of heulandite-group zeolites from the four groups are listed in Table 3 with one representative analysis per sample. One important EPMA result is that all the heulandite-group zeolites have a calcic composition. Nonframework cations are dominated by Ca+Mg (Figure 6). Thermal behaviors are reported in Table 3. The K contents are higher for samples with the thermal stability of clinoptilolite (43-89 and S-88-1) than for samples with an intermediate thermal behavior (90-16, S-88-2, S-88-3, 90-2a). This is in good agreement with the results of Alietti et al. (1974), Koyama and Takeuchi (1977) and Bish (1984) who showed that the thermal stability correlates with the K content.

Heulandite-group zeolites in groups 1, 2 and 3 have similar Si / (Al+Fe) ratios of 3.4–5.8 (Figure 7). The Mg content of heulandite-group minerals decreases from group 1 to 4. However, the heulandites from group 4 are rather different from all other heulandite-group minerals. The Si / (Al+Fe) ratios range from 2.4 to 3.2 (Figure 7) and Ca makes up 75–90% of the

Table 3. Representative electron microprobe analyses (wt. %) of glass (g) and heulandite-group minerals (hgm), Baucarit Formation, Sonora State, Mexico.

	Group 1		Group 2	Group 3				Group 4
Sample N°	90-16 g	90-16 hgm	S-88-2 hgm	S-88-3 hgm	90-2a hgm	43-89 hgm	S-88-1 hgm	90-8a hgm
SiO_2	77.40	66.49	67.21	67.23	67.88	68.41	68.52	58.26
Al_2O_3	13.00	13.20	13.40	12.77	13.01	12.51	12.24	18.54
FeO†	0.30	0.02	0.09	0.00	0.12	0.00	0.15	0.04
MgO	0.07	1.70	1.37	1.34	1.28	1.21	0.90	0.00
CaO	0.30	4.24	4.51	4.43	4.34	3.93	4.11	8.58
Na_2O	4.02	0.18	0.27	0.28	0.26	0.25	0.31	0.74
K_2O	5.20	0.77	0.79	0.97	0.80	1.63	1.30	0.58
Total	100.29	86.60	87.64	87.02	87.69	87.94	87.53	86.74
			Formula, 72 oxygen basis					
Si		29.18	29.19	29.40	29.40	29.62	29.78	26.29
Al		6.82	6.85	6.57	6.63	6.37	6.26	9.84
Fe		0.01	0.03	0.00	0.04	0.00	0.05	0.02
Mg		1.12	0.89	0.88	0.83	0.79	0.59	0.00
Ca		1.99	2.10	2.08	2.01	1.82	1.91	4.15
Na		0.15	0.23	0.24	0.22	0.21	0.26	0.65
K		0.43	0.44	0.54	0.44	0.90	0.72	0.33
Si/(Al + Fe)		4.28	4.24	4.47	4.41	4.65	4.72	2.67
Si + Al + Fe		36.01	36.07	35.97	36.07	35.99	36.10	36.15
E%		0.08	3.00	−1.76	4.37	0.69	4.60	6.10
Thermal behavior‡		I	I	I	I	I + C	C	H

† Fe total as Fe_2.

‡ Thermal behaviour refers to change in X-ray powder diffraction after heating at 450°C for 15 hr. C = clinoptilolite; I = intermediate heulandite; H = heulandite (Mumpton 1960).

https://doi.org/10.1346/CCMN.1996.0440105 Published online by Cambridge University Press

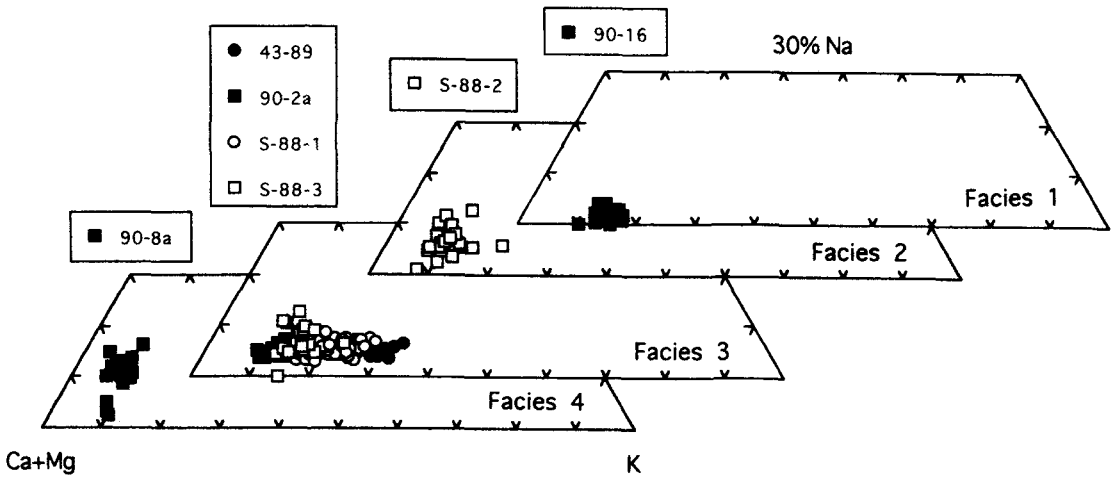

Figure 6. Triangular diagrams showing ratios of exchangeable cations in heulandite-group minerals from zeolitized tuffs within the Báucarit Formation, Sonora State, Mexico.

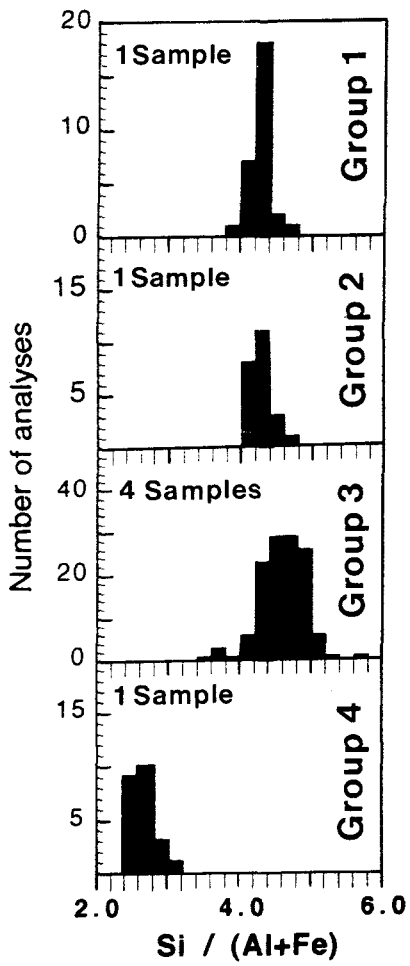

Figure 7. Histograms comparing distribution of Si/(Al + Fe) ratios for heulandite-group minerals from zeolitized tuffs within the Báucarit Formation, Sonora State, Mexico.

non-framework cations (Figure 6). Compared to heulandite-group zeolites in all other samples, they are Si and Mg depleted and enriched with Ca.

AEM RESULTS—CLAY CHEMISTRY. EDS analyses were performed on individual clay particles that were identified using morphology and SAED patterns for samples prepared from water suspension, and using lattice fringe images for ultra-thin sections of embedded clays. Great care was taken to analyze the different, texturally characterized areas. The structural formula were calculated for each analysis by normalization to 11 oxygens for example half cell for 2/1 clays. Chemical data are presented in Table 4 and illustrated in Figure 8.

Group 1 (sample 90-16) is characterized by clays with variable octahedral compositions and charge distributions. They range from Al-montmorillonites with a high Si content and a mean octahedral charge of 0.3 (Table 4), to an Fe-rich dioctahedral smectite (nontronite) characterized by lower Si and a higher layer charge, which is essentially compensated by K in the interlayer (Table 4). The Fe appears to be positively correlated with the K in the nontronitic smectites. The aluminous compositions correspond to the areas with typical smectite texture, whereas the ferric ones correspond to areas of illitic texture. There is a continuous variation between the aluminous and ferric analyzed end-members (Figure 8). The intermediate compositions can be interpreted as mixtures of variable proportions for the two end-members and have not been used to calculate the average composition of the two end-members (Table 4).

In samples of group 2, and only in those from this group, numerous analyses have been discarded because Si exceeded 4 for the tetrahedral sites. These high Si values are due to a mixing of smectite with

https://doi.org/10.1346/CCMN.1996.0440105 Published online by Cambridge University Press

Table 4. Structural formula ($O_{10}(OH)_2$) of clay minerals, based on the analytical transmission electron microscopy analyses.

Sample #		90-16		S-88-6	S-88-2	
Analyzed particle		Al-sm 2	Nontr. 6	Al-sm 6	Al-sm 5	Fe-sm 2
Tetrahedral	Si IV	3.98 (0.03)‡	3.62 (0.06)	3.89 (0.06)	3.98 (0.02)	4.00 (0.00)
site	Al IV	0.02 (0.03)	0.38 (0.06)	0.11 (0.06)	0.02 (0.02)	0.00 (0.00)
charge		0.02	0.38	0.11	0.02	0.00
Octahedral	Al VI	1.30 (0.11)	0.69 (0.20)	1.19 (0.08)	1.44 (0.14)	0.54 (0.05)
site	Fe	0.41 (0.18)	1.03 (0.24)	0.26 (0.17)	0.15 (0.12)	1.07 (0.01)
	Mg	0.31 (0.20)	0.28 (0.06)	0.70 (0.16)	0.56 (0.07)	0.51 (0.04)
charge		0.25	0.28	0.25	0.11	0.15
occupancy		2.02	2.00	2.15	2.15	2.12
Interlayer	Ca	0.04 (0.02)	0.10 (0.04)	0.04 (0.05)	0.06 (0.01)	0.07 (0.01)
site	K	0.21 (0.07)	0.45 (0.06)	0.20 (0.14)	0.01 (0.01)	0.02 (0.03)
charge		0.29	0.65	0.28	0.13	0.16

Sample #		90-2a		43-89			90-8a	
Analyzed particle		Al-sm 3	Mg, Fe-sm 3	Al-sm 3	Mg, Fe-sm 5	illite 7	Al-sm 4	Mg, Fe-sm 2
Tetrahedral	Si IV	3.93 (0.05)	3.88 (0.03)	3.74 (0.10)	3.93 (0.07)	3.39 (0.08)	3.69 (0.15)	3.81 (0.07)
site	Al IV	0.07 (0.05)	0.12 (0.03)	0.26 (0.10)	0.07 (0.07)	0.61 (0.08)	0.31 (0.15)	0.19 (0.07)
charge		0.07	0.12	0.26	0.07	0.61	0.31	0.19
Octahedral	Al VI	1.23 (0.10)	0.68 (0.12)	1.62 (0.26)	0.46 (0.18)	1.62 (0.07)	1.40 (0.24)	0.95 (0.07)
site	Fe	0.30 (0.18)	0.61 (0.11)	0.20 (0.11)	0.84 (0.35)	0.19 (0.03)	0.40 (0.07)	0.52 (0.02)
	Mg	0.49 (0.07)	0.97 (0.06)	0.28 (0.23)	0.94 (0.25)	0.28 (0.05)	0.26 (0.20)	0.66 (0.09)
charge		0.43	0.19	0.02	0.22	0.01	0.08	0.27
occupancy		2.02	2.26	2.10	2.24	2.09	2.06	2.13
Interlayer	Ca	0.07 (0.03)	0.09 (0.01)	0.04 (0.04)	0.07 (0.05)	0.00 (0.00)	0.12 (0.02)	0.15 (0.01)
site	K	0.36 (0.22)	0.11 (0.06)	0.18 (0.11)	0.14 (0.09)	0.62 (0.02)	0.14 (0.05)	0.16 (0.08)
charge		0.50	0.29	0.26	0.28	0.62	0.38	0.46

† = Standard deviation.

relicts of the siliceous substrate. From high resolution images, smectites sometimes appear as rare layers, very fragile and disseminated, within an amorphous matrix. Thus, SAED patterns obtained on a 100 Å large area substantiate a turbostratic texture due to the disordered layers, but AEM analyses over the same area correspond to the mixture of smectite layers and amorphous material. The 100 Å large areas of lattice fringes, free of amorphous zones (Figure 3d) were chosen to obtain well balanced formula. Except for two analyses from sample S-88-2, the clays have a homogeneous composition. They are Al- and Si-rich (Figure 8). Their charge distributions (Table 4) correspond to Al-montmorillonite. Two analyses from sample S-88-2 have a different composition. They are Fe-rich with equal proportions of Al and Mg within the octahedral site (Figure 8 and Table 4), but with a charge distribution identical to Al-montmorillonites, which are Fe-montmorillonites.

Group 3 shows the most variable clay mineral composition. Three types of clays were identified by AEM that exhibit different morphologies on TEM images described previously. One type corresponds unambiguously to the X-ray identified illite. Its composition is Al dominant within the octahedral site with a charge distribution typical of illite (Figure 8, Table 4). These illites have a layer charge (0.51 ± 0.13); near the minimum permissible without leading to expandability (Bailey 1984). According to Srodon and Eberl (1984), this charge distribution would correspond to ordered illite/smectite instead of illite end-member, but lattice images did not confirm this conclusion. The observed octahedral Fe and Mg composition is quite similar to that of the mean illite given by Weaver and Pollard (1975). However, structural arguments shown by high-resolution images of layer structure seem to show that there are not only typical illites, rigid structure of parallel layers with 10 Å periodicity, but also slightly expandable illite, near 10.5 Å periodicity (Figure 4h). These illite layers were not interstratified with smectite layers.

The second and third clay types from group 3 correspond to smectites. There are great variations for the octahedral compositions (Figure 8) that are continuous between two end-members. The octahedral composition ranges from an Al-rich to a more Mg and Fe-rich end-member. The octahedral composition of the Mg and Fe-rich end-member varies slightly between Mg and Fe-dominant clays. Thus, it appears that there is a coupled substitution between Al and (Mg,Fe), as proposed by Güven (1988) for dioctahedral smectites. However, the octahedral occupancy (1.95 to 2.21) of the Al-dominant clays corresponds well to dioctahedral smectite, whereas that of the Mg and Fe-rich

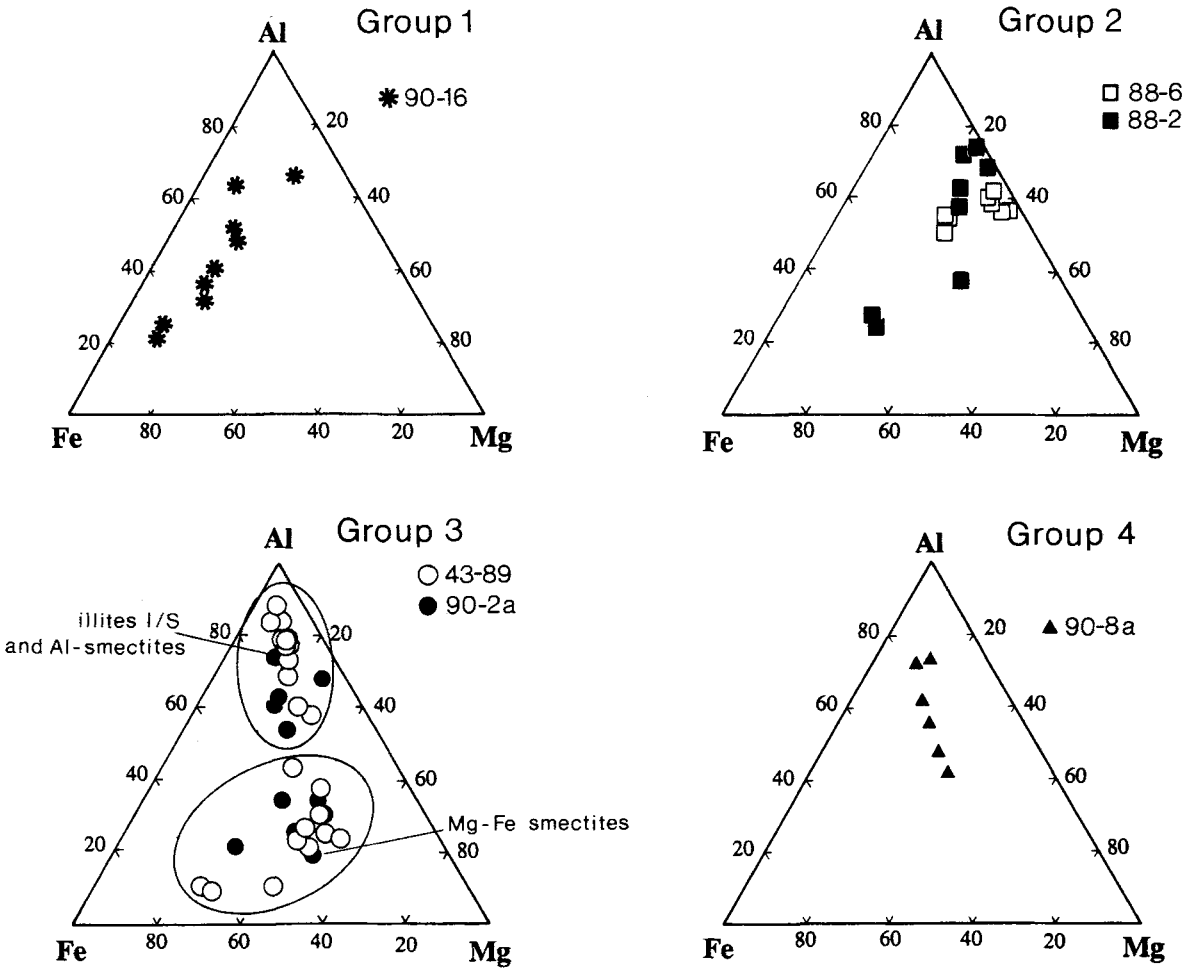

Figure 8. Octahedral compositions (Al : Mg : Fe) of clay minerals as calculated for normalized analyses.

smectites is higher (2.2 to 2.4) suggesting a tendency toward an intermediate di- and trioctahedral state. The tetrahedral substitution within aluminous and Mg and Fe-rich smectites is low (between 0.3 and 0 per half-cell). The K content of both smectites from this group is generally near 0.15 except for one analysis of aluminous smectite from sample 90-2a. For samples 43-89 as well as 90-2a, the chemical differences could be correlated with the morphology, Mg and Fe-dominant smectites are lath-shaped (Figure 4d), whereas Al-dominant smectites are flaky (Figure 4a). It is noted that only few particles have a charge distribution corresponding to randomly interstratified illite/smectite.

In group 4 (sample 90-8a), Al is always dominant within the octahedral site but it is quite variable. As for samples from group 3, there is a continuous variation between an aluminous and a more Mg and ferric octahedral composition. Unfortunately, we were unable to obtain reliable analysis of the Mg and Fe-rich end-member, but chemical analyses indicate a strong Mg-enrichment and a lower Fe-enrichment. The charge distribution correspond to tetrahedrally-charged clays like beidellites or randomly interstratified illite/smectite.

From AEM results, it is noticeable that different chemical features may be assigned to each type of morphology. Flaky clay particles with curled edges correspond to aluminous smectite for all of the studied samples. The very thin lath or ribbon shaped particles associated with the aluminous smectite particles correspond to nontronite in the sample 90-16 and to Mg-rich dioctahedral smectite in samples from groups 3 and 4. From samples of group 3, illites are well-crystallized subhedral or lathy particles.

One can notice a discrepancy between XRD and AEM data for samples from group 3. The XRD results indicate the presence of interstratified illite/smectite and discrete illite, whereas AEM data indicate smectites, illite and only few illite/smectite. The difference may be attributed to two reasons: 1) it is difficult to estimate the I/S illite layer content when the rate is low (<30%); and 2) the chemical differences between

https://doi.org/10.1346/CCMN.1996.0440105 Published online by Cambridge University Press

Table 5. Whole-rock analyses of altered tuffs within the Baucarit Formation, Sonora State, Mexico.

	Group 1	Group 2			Group 3				Group 4
Sample #	90-16	45-89	S-88-6	S-88-2	90-2a	S-88-3	S-88-1	43-89	90-8a
SiO_2	68.63	52.42	61.36	62.14	61.07	63.28	64.94	67.21	53.05
TiO_2	0.11	0.19	0.20	0.20	0.29	0.14	0.13	0.25	0.80
Al_2O_3	12.11	14.17	13.38	12.83	12.78	12.53	11.83	12.09	15.47
Fe_2O_3	0.88	0.98	1.42	1.11	1.68	1.07	1.05	1.54	5.55
FeO	0.17	0.08	0.09	0.09	0.25	0.09	0.09	0.08	0.22
MnO	0.07	0.03	0.02	0.02	0.05	0.05	0.07	0.07	0.08
MgO	1.06	6.19	2.50	1.82	1.80	1.48	1.18	1.33	2.91
CaO	3.04	2.23	3.52	4.36	4.44	4.55	3.97	2.52	5.00
Na_2O	1.16	0.35	1.22	0.42	0.88	0.20	0.39	1.21	0.87
K_2O	2.43	0.97	0.59	0.91	1.28	0.88	1.53	3.31	1.92
P_2O_5	0.11	0.11	0.04	0.02	0.13	0.01	0.01	0.12	0.27
H_2O+	8.05	8.00	10.92	10.37	11.00	10.02	8.72	7.75	9.25
H_2O-	2.75	14.00	4.85	5.12	3.82	5.17	4.92	2.72	4.90
Total	100.57	99.72	100.11	99.41	99.47	99.47	98.83	100.20	100.29

true smectite and random I/S with a high smectite layer rate cannot be resolved by AEM analyses due to analytical errors.

A limited number of samples has been analyzed from each group. Nevertheless, the clay mineralogy and composition clearly differ from the less altered samples that contained relict glass (90-16%) to the more altered samples (43-89 and 90-2a) where the glass was completely altered. At the first alteration stage, clays are Al- and Fe-rich montmorillonites with varying proportions of Al and Fe. In the next stage, Al-montmorillonite dominates but may contain significant amounts of Fe. In highly altered samples, smectites divide in two species, an Al-rich and a Fe- and Mg-rich montmorillonite, which are associated to illite.

WHOLE ROCK CHEMISTRY. The chemical compositions of the altered tuffaceous rocks interbedded within the Báucarit Formation are given in Table 5. Smectite-rich samples have high Al_2O_3 and MgO contents, whereas zeolite-rich tuffs have high SiO_2 and CaO contents. The high K_2O content of sample 43-89 is compatible with the presence of illite and potassic zeolites.

The chemical compositions of the altered tuffs have been compared with those of unaltered vitric rocks from the immediately underlying bimodal volcanic sequence. The rhyolitic composition for the volcanic glass from sample 90-16, and the presence of a small amount (<5%) of microphenocrysts of plagioclase, alkali feldspar, biotite and quartz indicate that the original composition of the studied samples may have been rhyolitic. Assuming that a uniform composition for the parent glass is not realistic, the tuff compositions have been normalized to that of 16 unaltered glassy rhyolites ranging from 68 to 72 wt% SiO_2 (data from Münch 1993; Delpretti 1987). These analyses are representative for the range of chemical composition found for the acidic rocks belonging to the bimodal mid-Tertiary volcanic sequence in central and eastern Sonora. This compositional range is assumed to represent that of the possible original compositions of the altered tuffs. Figure 9 is a graphic illustration of the ranges of relative enrichment or depletion. From this figure the following generalizations may be made: 1) Ca and Mg are strongly enriched during alteration; 2) Na and K are strongly depleted during alteration; and 3) Si and Al are generally retained, however Al is slightly enriched in clay-rich tuffs.

DISCUSSION

Timing of Alteration

The timing of alteration within the Báucarit Formation is poorly constrained but some field evidence is available. The sediments of the Báucarit Formation may have been indurated before they were faulted and tilted. This faulted/tilted deformation has been dated between 7–14 My for the Basin and Range province (Zoback et al. 1981). Moreover, the post-Báucarit sediments are poorly consolidated and they are generally zeolite-free. In Sonora, where zeolites have been observed, they are related to localized phenomena such as hydrothermal activity and alteration within closed hydrological systems (in close association with evaporites) and they generally do not belong to heulandite-group zeolites (J. Gonzalez-S 1993, written com.). Since deformation slightly postdates the deposition of the Báucarit Formation and since recent sediments are mainly non-zeolitized, one can infer that zeolitization within the sediments of the Báucarit Formation occurred soon after deposition.

Physico-chemical Environment of Alteration

CHEMICAL CHANGES DURING GLASS ALTERATION. As the original glass composition and the secondary phase compositions are known for sample 90-16, a mass balance calculation can be realized. This approach may

https://doi.org/10.1346/CCMN.1996.0440105 Published online by Cambridge University Press

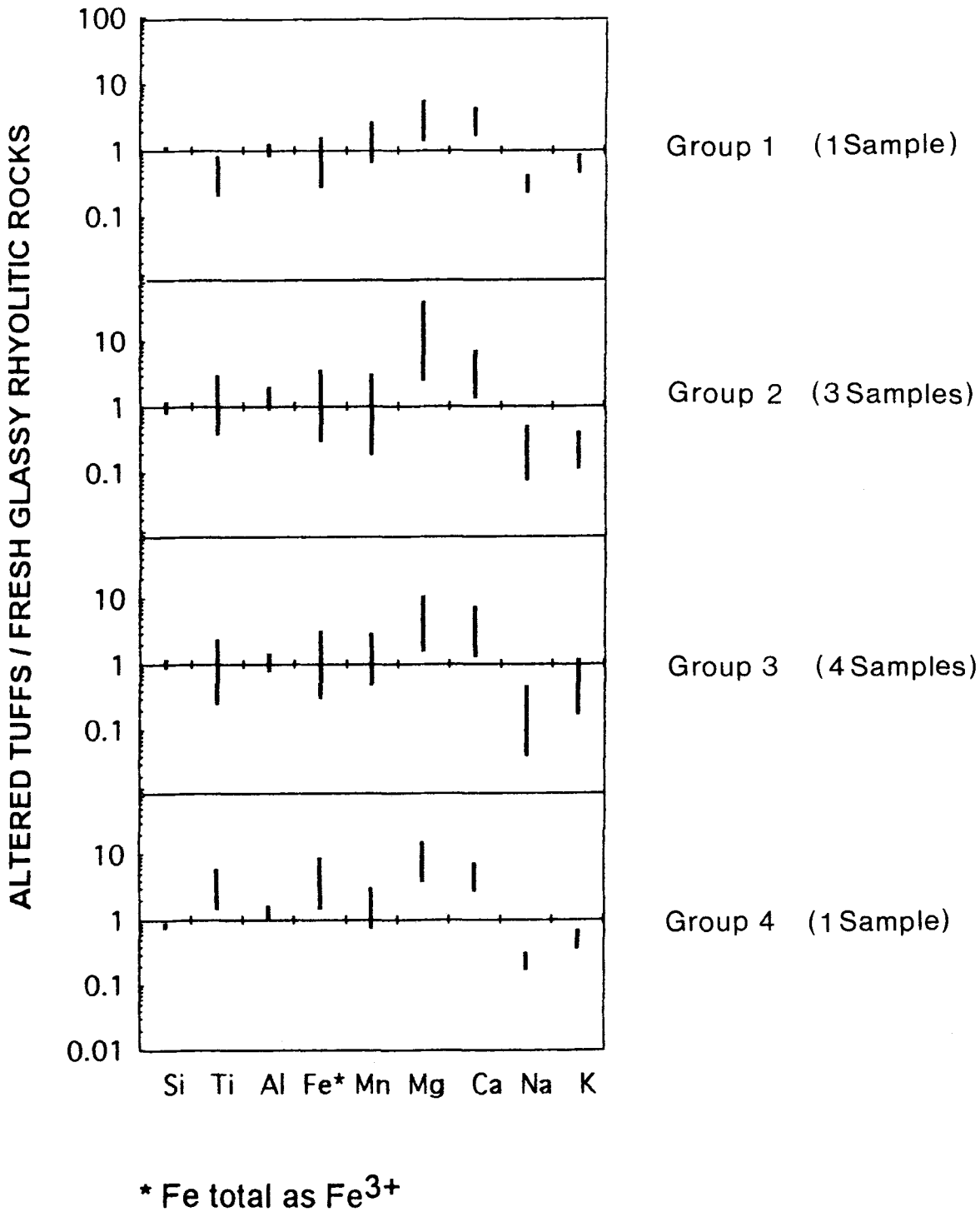

Figure 9. Logarithmic plot showing chemical differences between altered tuffs and fresh glassy rocks from Sonora State, Mexico. Major elements concentrations in altered tuffs (Table 5) are normalized to concentration in the 16 fresh glassy rhyolitic rocks with 68 to 72 wt% SiO_2. The bars represent the range of variation, taking into account the minimum and maximum of concentration of one element in 16 fresh rocks, the mean chemical composition of the altered rocks and analytical errors.

https://doi.org/10.1346/CCMN.1996.0440105 Published online by Cambridge University Press

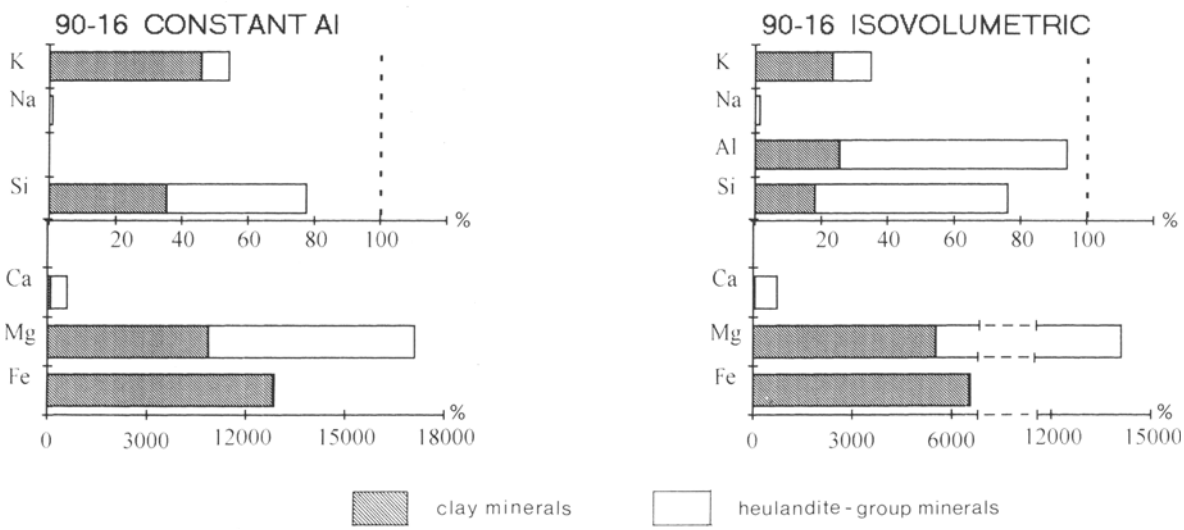

Figure 10. Mass balance results (isovolumetric and constant-Al calculations) for sample 90-16. Amounts of elements in alteration products are given in percent relative to the amount available from dissolved glass. Amounts below 100% indicate system loss. Totals above 100% indicate that these elements have to be externally added to the system.

give an idea of the mobility of elements and of the degree of aperture of the chemical system constituted by the tuff layer. The calculation was made following the method defined by Gresens (1967). From optical microscope, SEM observations and XRD analysis of bulk samples, the relative volumes of secondary phases used in calculations are 75% clay minerals and 25% zeolites. Densities have been measured using heavy liquids for glass (2.4 ± 0.1) and zeolites (2.15 ± 0.05) and have been taken from literature for smectites (2.05 ± 0.05) (Deer et al. 1962). We did not take into account the presence of opal as its relative volume was too difficult to estimate.

A mass balance has been calculated assuming a constant composition with respect to an insoluble element (Figure 10). This assumption allows for the volume of glass reacted to be estimated. From the relatively low solubility of Al, it is often assumed that Al does not migrate significantly during the alteration of glass to clay minerals and zeolites (Broxton et al. 1987; Altaner and Grim 1990). This is also supported by the results presented in Figure 9. For comparison, a second mass balance has also been calculated assuming an iso-volumetric alteration reaction (Figure 10). In such a case, the amount of glass altered is equivalent to the amount of secondary minerals.

The iso-volumetric calculation shows only a slight Al depletion, thus iso-volumetric and constant Al mass balances give similar results. Very large amounts of Na and K are lost by the system and Si is also depleted. The presence of opal, which indicates that the ground water was saturated with dissolved silica, may account for the lost silica in the mass balance calculations. Calcium, Mg and Fe are strongly enriched, with Mg showing the highest net system gain. Formation of the clay minerals accounts for all the Fe and about one-third of the Mg in the system, whereas the zeolite formation accounts for all the Ca and the largest amounts of Si, Al and Mg. If Al is held constant during the calculation, the secondary minerals assemblage would have to be 20% higher volume than the volume of the reacted glass.

The high net gains and losses of elements suggest that alteration has occurred under open system conditions. These high mass gains raise the question of the source of the dissolved Ca and Mg needed to form zeolites and Mg and Fe needed to form clay minerals. White et al. (1980) have shown that the dissolution of crystalline tuffs containing sanidine, quartz, biotite and clinopyroxene phenocrysts and sanidine-cristobalite groundmass resulted in solution enrichment of Ca, Mg and HCO_3. Thus, waters that have been circulating through volcaniclastic sediments and immediately underlying Tertiary acidic volcanic rocks from the bimodal sequence, might have been enriched with Ca and Mg. The source of Fe may still be controversial but Fe could have been dissolved from basic and intermediate rocks (basaltic andesites) belonging to the bimodal sequence. The depletion of Na and K is expected because of the high mobility of these elements. Alkalis are reported to migrate during hydration of glass (Arakami and Lipman 1965; Noble 1967) and they can readily be ion-exchanged into smectite and zeolite as shown by White et al. (1980).

FLUID COMPOSITIONS. The fluid compositions from which zeolites and associated clay minerals have precipitated is unknown, but an estimation can be made

https://doi.org/10.1346/CCMN.1996.0440105 Published online by Cambridge University Press

Table 6. Calculation of cation ratios and total dissolved species (TDS) of fluids from which clinoptilolite has precipitated.

	Group 1	Group 2	Group 3			
Sample N°	90-16	S-88-2	90-2a	S-88-3	S-88-1	43-89
K/Na/Ca/Mg (Mineral)	1/0.14/4.02/2.16	1/0.62/5.73/2.27	1/0.44/4.81/1.95	1/0.44/3.72/1.39	1/0.26/2.55/0.92	1/0.2/1.77/0.89
K/Na/Ca/Mg (Fluid)	1/11.2/201/118.8	1/49.6/286.5/124.9	1/35.2/240.5/107.3	1/35.2/186/76.45	1/20.8/127.5/50.6	1/16/88.5/49
log [(Na + K)/(Ca + Mg)] (Fluid)	−1.42	−0.91	−0.98	−0.86	−0.91	−0.9
TDS (Fluid)	<300 ppm	<300 ppm	<300 ppm	<300 ppm	<300 ppm	<300 ppm

using the method described by Boles and Surdam (1979). Fractionation factors between clinoptilolite and interstitial fluids defined by Boles and Wise (1978) have been applied to Ca-clinoptilolite as well as clinoptilolite and intermediate heulandite during this study in order to calculate mole proportions of K/Na/Ca/Mg in pore waters from those of Ca-clinoptilolite (Table 6). Using the calculated alkali/alkaline earth ratios, and chemical data from Jones (1965) for closed basin waters, the total dissolved species (TDS) of pore waters can be estimated (Boles and Surdam, Figure 7 1979). The calculated alkali/alkaline earth ratios and estimated TDS of pore waters from which Ca-clinoptilolite formed in vitric tuffs within the Báucarit Formation (Table 5) suggest that pore waters were relatively dilute (TDS < 300 ppm) and only slightly alkaline (log Na+K / Ca+Mg ranges from −1.4 to −0.4). However, these results are strongly dependent on the composition of the heulandite-group minerals that could either represent original compositions at the time of the zeolite formation or compositions later acquired by cation-exchange with interstitial pore fluids. Mass balance results, indicating a gain of volume in zeolitized tuffs, suggest a reduction of the porosity as zeolitization has proceeded. Consequently, the permeability of highly altered tuffs may have been greatly lowered restricting water mobility and the capacity of the zeolites to exchange cations with pore fluids. Thus, we propose that the heulandite-group minerals have retained their original calcic composition and have precipitated from relatively dilute and weakly alkaline waters.

OPEN VS CLOSED SYSTEM. Although the geological setting for the deposition of the Báucarit Formation, the block faulted and tilted region within the Basin and Range province, and the semi-arid climate of the region are appropriate for the development of closed hydrologic systems (Surdam 1978), the above results indicate that open system conditions have prevailed during alteration of vitric tuffs. For example: 1) no saline minerals (trona, halite, gaylussite) and no lateral zonation from fresh glass to analcime ± K-feldspar, both characterizing closed hydrological systems (Surdam 1978) have been observed within Miocene sediments; 2) Ca-clinoptilolite together with heulandite are uncommon alteration products for closed hydrological systems (Surdam 1978); 3) the high net mass gain and loss for mass balance results indicate that alteration has occurred within an open chemical system; and 4) the estimated fluid compositions in which Ca-clinoptilolites have formed correspond to that of relatively dilute and weakly alkaline waters.

The four groups of samples correspond to a progressive increase in glass alteration and they are concordant with an increase of relative depth of tuff layers within the sedimentary sequence. Thus, one can assume that a vertical zonation may occur within deposits of the Báucarit Formation. This assumption has to be considered very carefully because most samples come from different basins. However these mineral assemblages, and their reconstructed succession are similar to other occurrences for open systems of fresh and marine waters. For example, the Yucca Mountain, Nevada (Broxton et al. 1987); the Desatoya Mountains, Nevada (Barrows 1980); the Niigata oil field, Japan (Iijima and Utada 1971); the MITI-Kesennumaoki offshore borehole, Japan (Ogihara and Iijima 1989); and the Toa Baja borehole, Puerto Rico (Cho 1991). For the above examples, the alteration of vitric tuffs occurs in thick tuffaceous sequences and is enhanced by the local geothermal gradient and the burial depth whereas occurrences of tuff layers in the Báucarit Formation are scarce and the amount of burial is low. Moreover, burial diagenetic reactions occurred over a relatively wide range of depth for the above examples whereas the diagenetic zones in the Báucarit Formation should have been developed over a narrow range. Thus, it appears that the main controlling parameter during glass alteration within the Báucarit Formation (under open system conditions) was the temperature.

TEMPERATURE. The thermal conditions prevailing during alteration within the Báucarit Formation may be inferred from other environments. For burial diagenesis (or metamorphism) of silicic tuffs, Ca-clinoptilolite occurs at the lower part of zone II and can remain stable in zone IIIa characterized by the presence of

https://doi.org/10.1346/CCMN.1996.0440105 Published online by Cambridge University Press

heulandite (Iijima 1978, 1988; Ogihara and Iijima 1989). The lower stability temperature of the heulandite zone (zone IIIa) is about 84–91°C (Iijima 1978, 1988). At Toa Baja, the lower stability temperature of Ca-clinoptilolite has been estimated at 90°C, and the transition temperature between heulandite and laumontite zones at 125°C (Cho 1991). At Yucca Mountain, the boundary between the clinoptilolite and the analcime zone lies at an estimated temperature ranging from 100 to 150°C (Smyth 1982). Calcic zeolites such as heulandite are also characteristic of hydrothermal settings (Iijima 1988). Moreover, the calcic composition of all the heulandite-group zeolites is compatible with low temperature hydrothermal activity. At Wairakei geothermal area, New Zealand, the maximum temperature for heulandite stability is around 200°C (Coombs et al. 1959). In the Yellowstone hydrothermal environment, potassic clinoptilolite is stable to at least 140°C (Keith et al. 1978). Although the stability of the heulandite-group minerals is still controversial, heulandite was probably formed between 85 and 125°C and clinoptilolite at a slightly lower or similar temperature. The estimated geothermal gradient, based upon the above-cited temperatures and upon the maximum observed thickness for the Báucarit Formation (400 m), should be at least about 20°C/100 m.

Contribution of Clay Mineralogy (AEM Results)

From group 1 to 4, AEM results have pointed out variations in clay mineralogy within altered tuffs. Nontronitic smectites are restricted to sample 90-16, which represents the less altered tuff layer and is assumed to be at the uppermost level of the volcanosedimentary sequence. Aluminous montmorillonites are pervasive along the entire assumed sequence, but they are most abundant in samples with intermediate position, especially in samples from group 2. Mg and Fe-rich di-trioctahedral smectites are present in the deepest part of the sequence, and they have always been found coexisting with aluminous montmorillonites or beidellites.

Smectites from sample 90-16 are characterized by their high Fe content. However, the volcanic glass from which they originated is Fe-poor. This involves the solution supply and transport of Fe^{2+}, due to the very low solubility of Fe^{3+}, and reprecipitation as Fe^{3+} in nontronites. Such oxidizing conditions are compatible with the assumed position of this sample in the sedimentary sequence, allowing fresh oxygenated waters (probably meteoric in origin) to flush the tuff layer at shallow depth. Nontronites have been found stable in various settings, mainly for ocean floor hydrothermal settings and during weathering of basaltic rocks. Recently, they have been also described as weathering products of felsic volcanics (Banfield et al. 1991a). However, they are characteristic of dilute solution environments at relatively low temperature (Tardy et al. 1987). Nontronites or dioctahedral ferric smectites close to nontronites have been synthetized under reducing as well as oxidizing conditions, but at a higher temperature (100–150°C) in the latter case (Decarreau et al. 1987) than in the former which was 75°C (Decarreau and Bonin 1986). Moreover, in experimental hydrothermal alteration of an obsidian (300°C—100 MPa) Thomassin and Iiyama (1988) have shown that phyllosilicates (nontronite and beidellite) may precipitate from the reacted solution.

Within tuff layers from the next stage of glass alteration (group 2), only aluminous smectites, similar to those of sample 90-16, remain. However, the Mg content of these montmorillonites is higher than that of smectites from the less altered samples. Montmorillonite appears as a result of confined conditions when percolating solutions become concentrated by evaporation or long passage through sediments (Tardy et al. 1987). Thus, conditions appear to have changed between groups 1 and 2, and nontronite is no longer stable. Montmorillonites are stable in various environments and are generally characteristic of relatively low temperature alteration (<150°C).

For groups 3 and 4, TEM observations and AEM analyses suggest that aluminous smectites, similar to those from samples of group 2, have been partly replaced by ferromagnesium smectites. This reaction is accompanied by a morphological change, as lath-like particles developed at the expense of the flake-like particles. A study of smectite-to-illite transition by TEM and AEM analyses, Inoue et al. (1987) showed that randomly interstratified I/S minerals have a similar morphology (thin lath-shaped particles coexisting with dominant flake-like particles). Moreover, the Mg- and Fe-rich smectites having an octahedral occupancy (as high as 2.4) intermediate between a di- and trioctahedral state, the reaction of aluminous smectites with circulating fluids may have driven the aluminous smectites from the dioctahedral state toward an Mg and Fe enriched composition that retains a significant dioctahedral component (Banfield et al. 1991b). In a sedimentary environment, Mg is interpreted to be an indicator of the extent of diagenesis. Thus, Mg enrichment into clay minerals may be related to a change in fluid composition or to a higher concentration of the solution correlative with a decrease of the permeability, as Mg-rich clays like saponite are generally stable in concentrated environments (Tardy et al. 1987). As indicated by Jones (1986) and Jones and Weir (1983) for lacustrine clays, and from morphological and chemical variations, we propose that early-formed montmorillonites and beidellites may have come in contact with fluids and may have reacted with them to form the Mg, Fe-rich smectites. Consequently, we suggest that K fixation occurs but in ferromagnesium smectites rather than illite. Ferromagnesium smectites have already been described as a hydrothermal alter-

ation product of glassy rhyolitic tuffs from the Green Tuff Formation, in Japan (Kohyama et al. 1973) and from the Sierra Madre Occidental, in Chihuahua State, Mexico (Miranda 1980; Aniel 1983). Ferromagnesium smectites with apparently di-trioctahedral character have also been described as alteration products of basaltic rocks (Brigatti 1983; Danyak et al. 1980). As ferrous smectite is very unstable, the low layer charge of ferromagnesium smectite observed within samples from groups 3 and 4 could also be explained by some layer charge loss during post crystallization-oxidation. A similar explanation has been proposed by Güven (1988) for Mg, Fe-rich smectites with di-trioctahedral character described by Brigatti (1983) with almost similar composition to those observed here. He also suggested that these smectites could be partially altered celadonites based on the octahedral composition similarities.

Moreover for group 3, mainly sample 43-89, TEM and AEM analyses indicated the presence of subhedral illite crystals isolated from the smectite matrix. This illite is presumably similar to the authigenic discrete illite occurring within sandstones (Güven et al. 1980) or in hydrothermally altered shales (Yau et al. 1987, 1988). The subhedral shape of illite crystals suggests that crystallization occurs directly from an aqueous solution rather than by replacement of pre-existing phases (Yau et al. 1988). Yau et al. (1987) proposed that authigenic illite crystals could be derived from completely dissolved smectite under high water/rock ratio conditions for an active geothermal system. These conditions are compatible with the open-system alteration and the high net gains and losses indicated by our mass balance calculations and with the high thermal conditions inferred from the Ca-rich zeolites' temperature stability.

The occurrence of authigenic illite raises the problem of the interstratification of aluminous smectites with ferromagnesium smectites rather than illites. We suggest that illite crystallization occurred later than the formation of ferromagnesium smectites in remaining open pore-spaces and that both are related to circulating fluids. However, illite may have crystallized directly from hydrothermal fluids whereas ferromagnesium smectites may have formed from early-formed aluminous smectites, as suggested by textures and morphologies. The formation of ferromagnesium smectites rather than illite interstratified with aluminous smectites may have been controlled by the composition of fluids. Roberson and Lahann (1981) showed experimentally that Ca^{2+} and Mg^{2+} inhibit the smectite-to-illite reaction rate. Thus, Mg mobilization in the Báucarit Formation, suggested by clay minerals and zeolite chemistry, may have promoted the formation of the ferromagnesium smectites with di-trioctahedral character. The Mg content of zeolites is negatively correlated with that of smectites, suggesting that zeolites have precipitated from evolved fluids. It is not clear if ferromagnesium smectite could be oxidized celadonite, as proposed by Güven (1988). However, celadonitic clay minerals have been observed in the sandstones of the Báucarit Formation (Münch 1993) and mixed layer montmorillonite-celadonite was described as the alteration product of silicic glass in an active geothermal area, such as Upper Geyser Basin, Yellowstone National Park (Keith et al. 1978). Besse et al. (1981) described a similar evolution from ferric beidellites toward magnesium saponites in the case of the hydrothermal alteration of a hyaloclastic basaltic sequence in a marine environment. Those authors questioned the presence of celadonite rather than illite interstratified with smectites. Those clay minerals are mainly associated with clinoptilolite.

CONCLUSION

In the southwesternmost Basin and Range province, the alteration of Miocene volcaniclastic sediments is a widespread phenomenon (Münch and Cochemé 1993). This study of tuff layers, representing a more homogeneous material than the sedimentary rocks, gives clues to a better understanding of diagenetic features within the Báucarit Formation. The alteration of volcanic silicic glass within these tuffs seems to have occurred under open system conditions and at a rather elevated temperature (up to 125°C) with respect to their low burial amount (<400 m). The fluids that have interacted with volcanic glass seem to have been relatively fresh. At least, it appears that there is a positive correlation between the degree of glass alteration and the relative amount of burial.

Another goal of this study was to examine the clay mineralogy using electron microscopy. The main observed feature of clay mineralogy is that there is an evolution from aluminous smectites toward more magnesium compositions. This chemical evolution is accompanied by morphological changes of the clay minerals and is concordant with increasing glass alteration and with a progressive closure of the system. The clay minerals as well as zeolites, are also indicative of glass alteration at a low temperature (<125°C). Moreover, from chemical results, it appears that there is a chemical equilibrium between zeolites and smectites, which is consistent with a process of progressive pore spaces sealing during alteration. A similar process has been described at Yellowstone geothermal area and has been called hydrothermal self-sealing (Keith et al. 1978). Thus, we propose that volcanic glass within tuff layers has been altered, under high water/rock ratio conditions by relatively hot fluids. The Báucarit Formation may then have undergone a high temperature diagenesis in response to hot fluid circulations within the basins.

ACKNOWLEDGMENTS

Comments by D. Robinson and L. Aguirre are gratefully acknowledged. We thank R.L. Hay and B.F. Jones as well as the Editor-in-chief (Ray E. Ferrell, Jr.) for their constructive and thorough reviews. This work was supported by C.N.R.S.-I.N.S.U. grant D.B.T. 5-42 and E.E.C. grant CI1*-CT92-0044.

REFERENCES

Alietti A, Gottardi G, Poppi L. 1974. The heat behaviour of the cation exchanged zeolites with heulandite structure. Tschermacks Miner Petrogr mitt 21:291–298.

Altaner SP, Grim RE. 1990. Mineralogy, chemistry, and diagenesis of tuffs in the Sucker Creek formation (Miocene), Eastern Oregon. Clays & Clay Miner 38:561–572.

Aniel B. 1983. Les gisements d'uranium associés au volcanisme acide tertiaire de la Serra Pena Blanca (Chihuahua, Mexique). Thèse Doct., univ. Paris VI. 291p.

Arakami S, Lipman PW. 1965. Possible leaching of Na2O during hydration of volcanic glasses. Proc Jpn Acad 41: 467–470.

Bailey SW. 1984. Classification and structures of the micas. In: Bailey SW, editor. Micas. Reviews in Mineralogy, Mineral Soc Amer 13:1–12.

Banfield JF, Jones BF, Veblen DR. 1991a. An AEM-TEM study of weathering and diagenesis, Abert Lake, Oregon. 1. Weathering reactions in the volcanics. Geochim Cosmochim Acta 55:2781–2794.

Banfield JF, Jones BF, Veblen DR. 1991b. An AEM-TEM study of weathering and diagenesis, Abert Lake, Oregon. 2. Diagenetic modification of the sedimentary assemblage. Geochim Cosmochim Acta 55:2795–2810.

Barrows KJ. 1980. Zeolitization of Miocene volcaniclastic rocks, southern Desatoya Mountains, Nevada: Geol Soc Amer Bull P-1, 91:199–210.

Bartolini C, Morales M, Damon P, Shafiqullah M. 1992. K-Ar ages of tilted tertiary volcanic rocks associated with continental conglomerates, Sonoran Basin and Range Province, Mexico. Geol Soc Am, Cordilleran Section, Abstracts with Programs 24:6.

Besse D, Desprairies A, Jehannot C, Kolla V. 1981. Les paragenèses de smectites et de zéolites dans une série pyroclastique d'âge éocène moyen de l'Océan Indien (D.S.D.P., Leg 26, Site 253). Bull Miner 104:56–63.

Bish DL. 1984. Effects of exchangeable cation composition on the thermal expansion/contraction of clinoptilolite. Clays & Clay Miner 32:444–452.

Bockoven NT. 1980. Reconnaissance geology of the Yécora-Ocampo area, Sonora and Chihuahua, Mexico. Ph. D. Thesis, Univ. of Texas, Austin. 197 p.

Boles JR, Surdam RC. 1979. Diagenesis of volcanogenic sediments in tertiary saline lake; Wagon Bed Formation, Wyoming. Am J Sci 279:832–853.

Boles JR, Wise WS. 1978. Nature and origin of deep-sea clinoptilolite. In Sand LB, Mumpton FA, editors. Natural Zeolites, Occurrence, Properties, Use. Elmsford, New York: Pergamon Press. 235–243.

Brigatti MF. 1983. Relationships between composition and structure in Fe-rich smectites. Clay Miner 18:177–186.

Broxton DE, Bish DL, Warren RG. 1987. Distribution and chemistry of diagenetic minerals at Yucca Mountain, Nye County, Nevada. Clays & Clay Miner 35:89–110.

Cho M. 1991. Zeolite to prehnite-pumpellyite facies metamorphism in the Toa Baja Drill Hole, Puerto Rico. Geophys Res Lett 18:525–528.

Cliff G, Lorimer GW. 1975. The quantitative analysis of thin specimens. J Microsc 103:203–207.

Cochemé JJ, Demant A, Aguirre L, Hermitte D. 1988. Présence de Heulandite dans les remplissages sédimentaires liés au "Basin and Range"(Formation Báucarit) du nord de la Sierra Madre Occidentale (Mexique). C R Acad Sci Paris 307:II, 643–649.

Coombs DS, Ellis AJ, Fyfe WS, Taylor AM. 1959. The zeolite facies, with comments on the interpretation of hydrothermal syntheses. Geochim Cosmochim Acta 17:53–107.

Danyak LG, Drits VA, Kudryavtsev I, Simanovich IM, Slonimskaya MV. 1980. Crystallochemical specificity of trioctahedral smectite containing ferric iron, the secondary alteration of oceanic and continental basalts. Doklady Akademii Nauk SSSR 259:1458–1462.

Decarreau A, Bonin D. 1986. Synthesis and crystallogenesis at low temperature of Fe(III)-smectites by evolution of coprecipitated gels: experiments in partially reducing conditions. Clay Miner 21:861–877.

Decarreau A, Badaut-Trauth D, Couty R, Kaiser P. 1987. Synthesis and crystallogenesis of ferric smectite by evolution of Si-Fe coprecipitates in oxidizing conditions. Clay Miner 22:207–223.

Deer WA, Howie RA, Zussman J. 1962. Sheet silicates. In: Rock-Forming Minerals. New York:J. Wiley & Sons. 270p.

Delpretti P. 1987. Contribution à l'étude de la Sierra Madre Occidentale (Mexique): la séquence volcanique tertiaire de la transversale Tepoca-Yepachic. Thèse Doct., Univ. Aix-Marseille III. 344 p.

Demant A, Cochemé JJ, Delpretti P, Piguet P. 1989. Geology and petrology of the Tertiary volcanics of the northwestern Sierra Madre Occidental, Mexico. Bull Soc Géol Fr (8) 5: 737–748.

Drewes HD. 1981. Tectonics of southeastern Arizona. U.S. Geol Surv Prof Pap 1144.

Gonzales SJ. 1993. University of Sonora, Hermosillo, Mexico:personal communication.

Gresens RL. 1967. Composition-volume relationship of metasomatism. Chem Geol 2:47–65.

Güven N. 1988. Smectites. In:Bailey SW, editor. Hydrous phyllosilicates (exclusive of micas). Reviews in Mineralogy, Mineral Soc Am 19:497–552.

Güven N, Hower WF, Davies DK. 1980. Nature of authigenic illites in sandstone reservoirs. J Sed Petrol 50:761–766.

Iijima A. 1978. Geologic occurrences of zeolites in marine environments. In: Sand LB, Mumpton FA, editors. Natural zeolites: Occurrence, Properties, Use. Elmsford, New York: Pergamon Press. 175–198.

Iijima A. 1988. Diagenetic transformations of minerals as exemplified by zeolites and silica minerals -a Japanese view. In: Chilingarian GV, Wolf KH, editors. Diagenesis II. Amsterdam:Elsevier. 147–211.

Iijima A, Utada M. 1971. Present-day zeolitic diagenesis of the Neogene geosynclinal deposits of the Niigata oil field, Japan. In: Molecular sieve zeolites I. Am Chem Soc Adv Chem Ser 101:342–349.

Inoue A, Kohyama N, Kitagawa R, Watanabe T. 1987. Chemical and morphological evidence for the conversion of smectite to illite. Clays & Clay Miner 35:111–120.

Jones BF. 1965. The hydrology and mineralogy of Deep Springs Lake, Inyo County, California. U.S. Geol Surv Prof Pap 502-A: 56p.

Jones BF. 1986. Clay mineral diagenesis in lacustrine sediments. In: Mumpton FA, editor. Studies in diagenesis. U.S. Geol Surv Bull 1578:291–296.

Jones BF, Weir AH. 1983. Clay minerals of lake Abert, an alkaline, saline lake. Clays & Clay Miner 31:161–172.

Keith TEC, White DE, Beeson MH. 1978. Hydrothermal alteration and self-sealing in Y-7 and Y-8 drill holes in northern part of Upper Geyser Basin, Yellowstone National Park, Wyoming. U.S. Geol Surv Prof Pap 1054-A: A1–A26.

Keller WD, Reynolds RC, Inoue A. 1986. Morphology of clay minerals in the smectite-to-illite conversion series by scanning electron microscopy. Clays & Clay Miner 34: 187–197.

King RE. 1939. Geological reconnaissance in northern Sierra Madre Occidental of Mexico. Geol Soc Am Bull 50:1625–1722.

Kohyama N, Shimoda S, Sudo T. 1973. Iron-rich saponite (ferrous and ferric forms). Clays & Clay Miner 21:229–237.

Koyama K, Takeuchi Y. 1977. Clinoptilolite: the distribution of potassium atoms and its role in thermal stability. Z Kristallogr 145:216–239.

Miranda M. 1980. Geoquimica de sedimentos de arroyo del districto uranifero. Sierra de Pena Blanca Chihuahua. URAMEX private Dept. 47p.

Mumpton FA. 1960. Clinoptilolite redefined. Am Mineral 45:351–369.

Münch P. 1993. Pétrologie et géochimie des tufs et des roches volcano-détritiques des bassins Miocènes dans la région du Sonora, Mexique: contribution à l'étude du métamorphisme de trés bas degré en contexte distensif. Thèse Univ. Aix-Marseille III. 225p.

Münch P, Cochemé JJ. 1993. Heulandite-group zeolites in volcaniclastic deposits of the southern Basin and Range province, Mexico. Eur J Min 5:171–180.

Noble DC. 1967. Sodium, potassium, and ferrous iron contents of some secondarily hydrated natural silicic glasses. Am Mineral 52:280–286.

Ogihara S, Iijima A. 1989. Clinoptilolite to heulandite transformation in burial diagenesis. In: Jacobs PA, van Santen RA, editors. Zeolites: Facts, Figures, Future. 491–500.

Passaglia E. 1970. The crystal chemistry of chabazites. Am Miner 55:1278–1301.

Rettke RC. 1981. Probable burial diagenetic and provenance effects on Dakota group clay mineralogy, Denver basin. J Sed Petrol 51:0541–0551.

Roberson HE, Lahann R. 1981. Smectite to illite conversion rates: effects of solution chemistry. Clays & Clay Miner 29:129–135.

Smyth JR. 1982. Zeolite stability constraints on radioactive waste isolation in zeolite-bearing volcanic rocks. J Geol 90: 195–201.

Srodon J, Eberl DD. 1984. Illite. In: Bailey SW, editor. Micas. Reviews in Mineralogy 13, Mineral Soc Am 495–544.

Surdam RC. 1978. Zeolites in closed hydrologic systems. In: Mumpton FA, editor. Mineralogy and geology of natural zeolites. Reviews in Mineralogy 4. Washington, D.C.: Mineral Soc Am 65–91.

Tardy Y, Duplay J, Fritz B. 1987. Stability fields of smectites and illites as a function of temperature and chemical composition. In: Proc Internat Meeting "Geochemistry of the Earth Surface and Processes of Mineral Formation", Granada. 461–494.

Thomassin JH, Iiyama JT. 1988. Etude expérimentale des stades précoces de l'altération hydrothermale de matériaux vitreux: cas d'une obsidienne (300°C —100MPa). Bull Minéral 111:633–647.

Weaver E, Pollard LD. 1975. The chemistry of clay minerals. Developments in Sedimentology 15. Amsterdam:Elsevier. 213p.

Weir AH, Ormerod EG, El Mansey IMI. 1975. Clay mineralogy of sediments of the western Nile Delta. Clay Miner 10:369–386.

White AF, Claassen HC, Benson LV. 1980. The effect of dissolution of volcanic glass on the water chemistry in a tuffaceous aquifer, Rainier Mesa, Nevada. U.S. Geol Surv Water-Supply Pap 1535-Q. 34 p.

Yau Y-C, Peacor DR, McDowell SD. 1987. Smectite-to-illite reactions in Salton sea shales: a transmission and analytical electron microscopy study. J Sed Petrol 57:335–342.

Yau Y-C, Peacor DR, Beane RE, Essene EJ. 1988. Microstructures, formation mechanisms, and depth-zoning of phyllosilicates in geothermally altered shales, Salton sea, California. Clays & Clay Miner 36:1–10.

Zoback ML, Anderson RE, Thompson GA. 1981. Cenozoic evolution of the state of stress and style of tectonism of the Basin and Range province of the western United States. Phil Trans R Soc Lond 300:407–434.

(Received 27 July 1993; accepted 23 May 1995; Ms. 2406)